Effect of the beam-beam interactions on the dynamic aperture and amplitude growth in the LHC

T. Sen *, N. Gelfand, C. Johnstone, W. Wan, FNAL, Batavia, IL 60510

Abstract

The dynamic aperture at collision energy is determined primarily by the nonlinear fields of the IR quadrupoles but is also influenced by the beam-beam interactions. We revisit the choice of the crossing angle that maximizes the dynamic aperture with an accurate modeling of the long-range interactions and use of the present values of the IR quadrupole field harmonics. A separate but related issue we address is the amplitude growth of particles in the beam halo due to the long-range interactions.

1 INTRODUCTION

In this note our aim is to understand two issues: a) the relative importance of triplet nonlinearities and the beam-beam interaction in determining the dynamic aperture at collision energy and b) the effect of the long-range beam-beam interactions on amplitude growth of particles in the beam halo.

Previous studies of the first issue [1] have treated the long-range interactions in an approximate fashion. These assumptions have included i) neglecting the phase advance between long-range kicks, ii) assuming the beams are round at the locations of the long-range kicks, and iii) assuming that the dimensionless separation between the beams stays constant at all the kicks. All of these assumptions tend to over emphasize the strength of the long-range kicks. We have not made any of these approximations in our study. As a result we hope to have a more accurate assessment of parameters such as the optimal crossing angle given the knowledge of the triplet error harmonics. We use the program TEVLAT [2] to calculate the dynamic aperture when tracking for large numbers of turns and we also use MAD [3] for shorter term tracking to provide an independent check.

The second issue is important because the several long-range interactions in the LHC may scrape off particles in the tails of a given beam when these particles are close to the core of the other beam. This problem requires a statistical approach with a sufficiently large number of particles in the beam distribution. It is best studied by modelling all the beam-beam interactions accurately and ignoring the nonlinearities so that the effects of the beam-beam interactions on the distribution in the tails may be followed for a large number of turns. We have written such a code and we use it here for estimating the upper stability limit in the LHC at collision.

* email: tsen@fnal.gov

n	Normal $[\langle b_n\rangle, db_n, \sigma(b_n)]$ FNAL2/KEK2	Skew $[\langle a_n\rangle, da_n, \sigma(a_n)]$ FNAL2/KEK2
3	0, .3, .8/0, .51, 1.0	0, .3, .8/0, .51, 1.0
4	0, .2, .8/0, .29, .57	0, .2, .8/0, .29, .57
5	0, .2, .3/0, .19, .38	0, .2, .3/0, .19, .38
6	0, .6, .6/0, .5, .19	0, .05, .1/0, .10, .19
7	0, .06, .06/0, .05, .06	0, .04, .06/0, .05, .06
8	0, .05, .05/0, .02, .03	0, .03, .04/0, .02, .03
9	0, .03, .03/0, .01, .01	0, .02, .02/0, .01, .01
10	0, .03, .03/-0.25, .03, .01	0, .02, .03/ 0, .01, .01

Table 1: Design field harmonics, at a reference radius of 17mm, of the IR quadrupoles to be built at FNAL and KEK. Harmonics are expressed in units of 10^{-4}.

2 TRIPLET ERRORS AND TRACKING DESCRIPTION

At top energy the dominant nonlinearities in the machine are those of the IR quadrupoles. Considerable effort has gone into the design of these magnets both at Fermilab and KEK to ensure that the nonlinear harmonics stay within tolerable bounds. These errors have different sources: the low order harmonics are primarily due to fabrication errors and variations in coil size while the higher order harmonics are mainly due to measurement errors. In the target tables specified by the two laboratories, the errors are split into three parts: systematic errors $\langle b_n\rangle, \langle a_n\rangle$, uncertainties in the systematics db_n, da_n and random variations in the errors $\sigma(b_n), \sigma(a_n)$. These error tables have been refined and updated as measurements of more model magnets (5 at Fermilab, 2 at KEK so far) have become available. The studies reported here are based on error tables V2.0 (shown in Table 1) of the Fermilab and KEK magnets.

The lattice used in our tracking is derived from the MAD lattice version 5.1. Lattice nonlinearities are the IR quadrupole fields and chromaticity correcting sexupoles. In most of the calculations reported here, the systematic errors and the random errors of the body harmonics are included but not the uncertainties in the systematic errors. Earlier studies [4] had shown that these uncertainties reduced the dynamic aperture by about 0.5-1σ. Errors in the ends of the triplets are not included. For studies without the beam-beam interaction we have used 100 seeds for the random errors chosen from a Gaussian distribution. With the

beam-beam interaction we have used up to 5 random seeds. The physical aperture of the IR quadrupoles is represented in the tracking studies by aperture restrictions at $\pm$30mm. Misalignment errors are not included nor have any nonlinear correctors been used in these studies. As mentioned earlier, TEVLAT and MAD are used for tracking for 10^3 turns, both with and without the beam-beam interactions, to provide consistency checks and only TEVLAT has been used for tracking for 10^5 and 10^6 turns.

3 DYNAMIC APERTURE WITHOUT BEAM-BEAM INTERACTIONS

Extensive sets of simulations were done to calculate the dynamic aperture without the beam-beam interactions. Initially, Fermilab error tables were used for the triplet fields at both IR1 and IR5. Averaged over the 100 random seeds and over emittance space, the dynamic aperture after tracking for 1000 turns is $(11.2 \pm 1.7)\,\sigma$. At the low-end tails of the distribution, the dynamic aperture is $\sim$ 6-7σ. Amongst the individual multipoles, the octupole components (b_4, a_4) have a significant contribution to the variations of the dynamic aperture from seed to seed.

The first version of the KEK harmonics had a large systematic value of $\langle b_{10} \rangle = -1.0$. This multipole was found to reduce the dynamic aperture by about 2σ. This prompted a design change and version 2 of the KEK harmonics had a reduced value of $\langle b_{10} \rangle = -0.25$. Subsequently there was a proposal to mix the positioning of the magnets so that at both IR1 and IR5, the inner magnets of each triplet (Q2a, Q2b) would be Fermilab magnets and the outer magnets (Q1, Q3) would be KEK magnets. The dynamic aperture was calculated both in the unmixed and mixed case and the results are summarized in Table 3. Mixing the magnets increases the dynamic aperture by 0.6σ compared to the unmixed case. Figure 1 shows a histogram of the dynamic aperture (averaged over emittance space) calculated for 100 seeds. Figure 2 shows the dynamic aperture, averaged over the seeds, at each of the ten emittance ratios chosen as the initial conditions. Close to the vertical axis, the dynamic aperture is smaller which we attribute to the fact that the vertical tune is closer to the third order resonance.

ϕ	$\langle DA \rangle \pm \sigma_{\langle DA \rangle}$	
(μrad)	TEVLAT	MAD
100.0	15.0 ± 0.9	13.8 ± 1.1
200.0	13.8 ± 0.8	12.9 ± 1.2
300.0	11.7 ± 1.2	11.6 ± 1.6

Table 2: Dynamic aperture with mixed magnets, calculated after 1000 turns with TEVLAT and MAD at different crossing angles. The averages are over emittance space and over 20 random seeds.

TEVLAT tracking results were compared to results obtained using MAD for the mixed magnets scenario. The comparison was done for three different crossing angles.

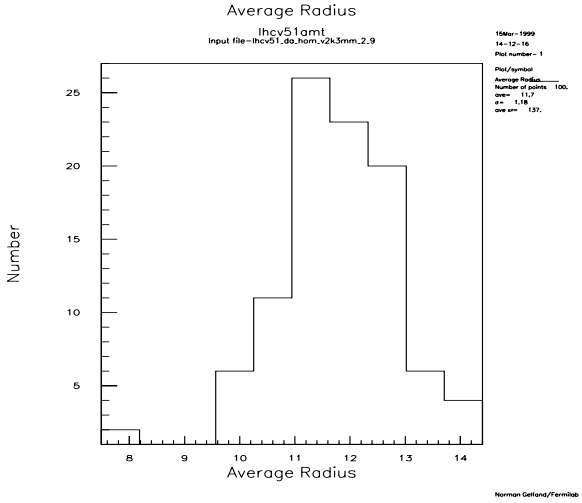

Figure 1: Distribution of the dynamic aperture with mixed magnets and errors shown in Table 1 over 100 seeds for the random errors. Particles were tracked for 1000 turns.

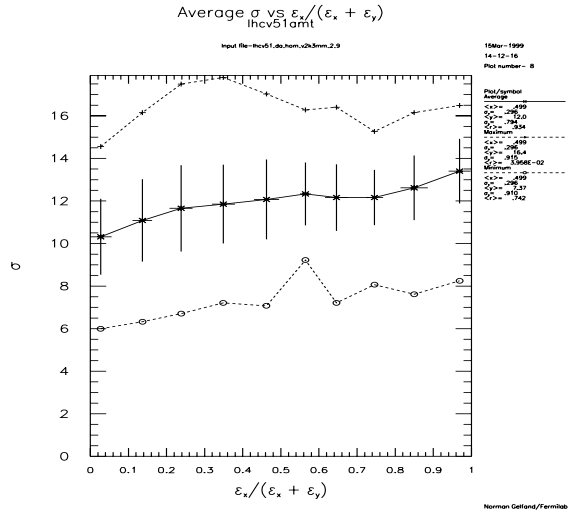

Figure 2: Dynamic aperture vs $\epsilon_x/(\epsilon_x + \epsilon_y)$ for the same cases as in Figure 1. The upper and lower curves represent the maximum and minimum values over 100 seeds.

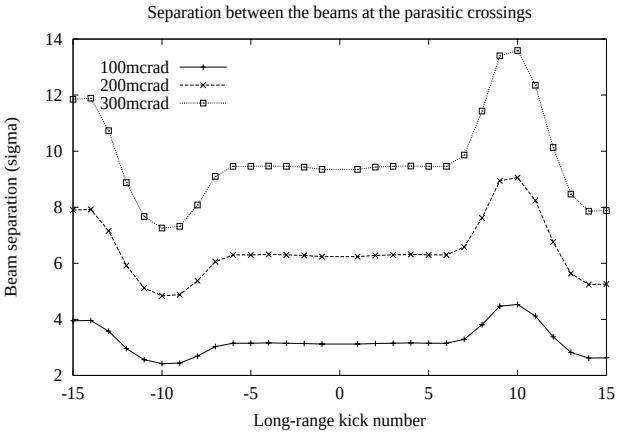

Figure 3: The separation between the two beams at each of the 30 parasitic crossings in a high luminosity IR for total crossing angles of 100, 200 and 300 μrad. The separation, measured in units of the rms size of a beam, stays constant within the drift section (kicks from -6 to +6) but varies within the triplet quadrupoles.

Two different distributions of 20 random seeds were used with TEVLAT and MAD. Table 2 shows that the results from the two codes are within 1 σ of each other. Some of these differences may be due to the use of different seeds.

4 DYNAMIC APERTURE WITH BEAM-BEAM INTERACTIONS

The major issue in including the beam-beam interactions is the treatment of the long-range interactions. Earlier studies had made approximations mentioned earlier in order to reduce the tracking time. While physically reasonable, these approximations are somewhat uncontrolled. For example, Figure 3 shows that the separation between the beams at a crossing angle of 300μrad varies between 7.8σ to 13.6σ and stays constant (at 9.5σ) only in the drift section. On the other hand, the phase advance between the kicks changes in the drift section but stays constant thereafter. We have not made these approximations in our models.

Initially the dynamic aperture with beam-beam interactions was calculated with 1000 turn tracking using both TEVLAT and MAD at crossing angles between 100 to 300μrad. This short term tracking with both codes showed that the dynamic aperture decreased as the crossing angle increased. This implies that over the short term, triplet errors dominate the effects due to the beam-beam interactions. We repeated the calculations with longer term tracking using TEVLAT. Compared to the short term tracking, the variation of the dynamic aperture with crossing angle is completely different over longer time scales. Figure 4 shows the results obtained with 10^5 and 10^6 turns tracking. After 10^5 turns, the dynamic aperture at 100μrad is less than 3σ (comparable to the minimum separation between the beams), increases to about 10σ at 300μrad before falling slightly at 350μrad. The calculations over 10^6 turns show that the dynamic aperture is nearly constant at about 6σ in the range from 300-400μrad.

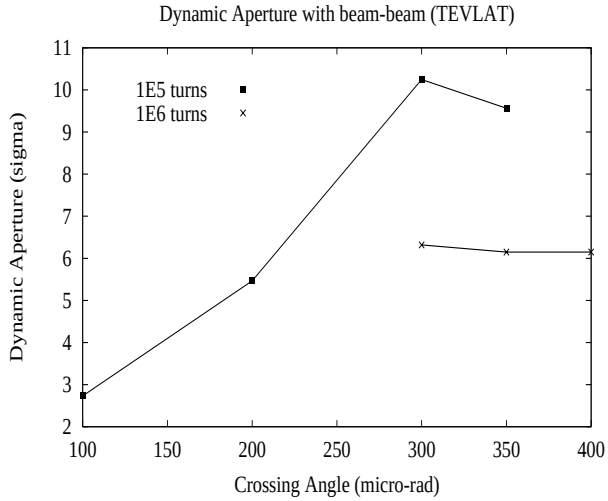

Figure 4: Dynamic aperture with beam-beam at different crossing angles. Particles were launched along the diagonal in emittance space. For 10^5 turns tracking, the crossing angle was varied between 100 to 350μrad and one seed was used for the random errors. For 10^6 turns tracking, the crossing angle was varied between 300 to 400μrad and 2 random seeds were used. This longer term tracking shows that the dynamic aperture is relatively flat at around 6σ in the range between 300-400μrad.

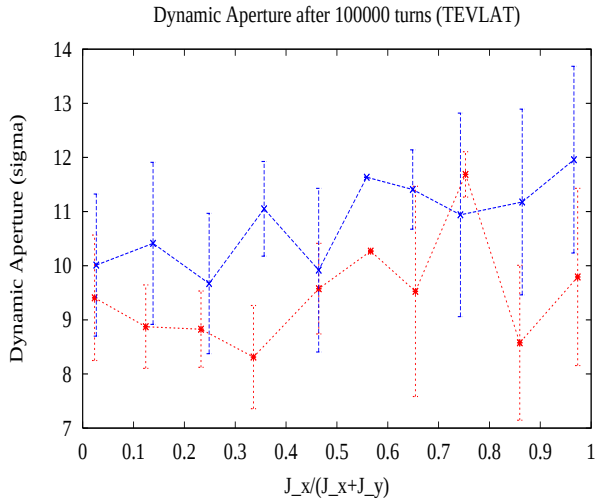

Figure 5: Dynamic aperture at a crossing angle of 300μrad both without the beam-beam interactions(blue) and with the beam-beam interactions (red). Particles were launched at 10 different angles in emittance space and tracked for 10^5 turns. 5 seeds were used for the random errors. The data points and error bars represent the averages and the standard deviations respectively.

Errors	BB	$\langle DA \rangle \pm \sigma_{\langle DA \rangle}$ Turns 10^3	Turns 10^5
FNAL everywhere	Off	11.2 ± 1.7	
KEK(IR1) & FNAL(IR5)			
KEK $\langle b_{10} \rangle$=-1.0	Off	9.0 ± 0.9	
KEK $\langle b_{10} \rangle$=-0.25	Off	11.1 ± 1.1	
KEK & FNAL (mixed)			
KEK $\langle b_{10} \rangle$=-0.25	Off	11.7 ± 1.2	10.8 ± 0.8
KEK $\langle b_{10} \rangle$=-0.25	On	11.0 ± 1.1	9.5 ± 1.0

Table 3: Summary of dynamic aperture calculations without and with the beam-beam (BB) interactions. For 1000 turn tracking, the dynamic apertures are calculated over 100 random seeds and averaged over the seeds and emittance space. For 10^5 turn tracking, 5 random seeds were used and the results also averaged over emittance space and the seeds.

The results shown in Figure 4 were obtained with particles tracked along the diagonal in emittance space and either one or two random seeds were used. A better estimate requires a larger sampling of both the orientations in emittance space and distributions of random errors. Figure 5 shows the dynamic aperture at a crossing angle of 300μrad at different angles in emittance space averaged over five random seeds and calculated over 10^5 turns both with and without the beam-beam interactions. Results for the average dynamic aperture are summarized in Table 3. Comparing the dynamic aperture with and without the beam-beam interactions seed by seed for a proper statistical analysis shows that the average drop in dynamic aperture due to the beam-beam after 10^5 turns is 1.4σ. The standard deviation on this average difference is 0.4σ.

5 GROWTH OF PARTICLES IN THE TAILS

The long-range interactions are expected to influence the amplitude growth of particles in the tails more than that of particles in the core. In the crossing plane, particles in the tails on one side of the bunch center will be close to the core of the other beam and will get a strong kick. On the other side of the IP and a phase advance π away, these particles will again be close to the core of the other beam so they will experience strong beam-beam kicks both upstream and downstream of the IP.

In order to understand the effects of the long-range interactions we have written a separate program. Features of this code include: i) six dimensional motion, including synchrotron oscillations, ii) thin lens beam-beam kicks, including energy kicks a la Piwinski, iii) longitudinal slicing of the strong beam for the head-on interaction, iv) exact treatment of the long-range kicks, v) the lattice is represented by a linear map, vi) tune and offset modulation and noise, vii) PACMAN bunches can be studied. Future additions that are planned include approximations of the complex error functions to speed up the code and the addition of multipole kicks from the triplets.

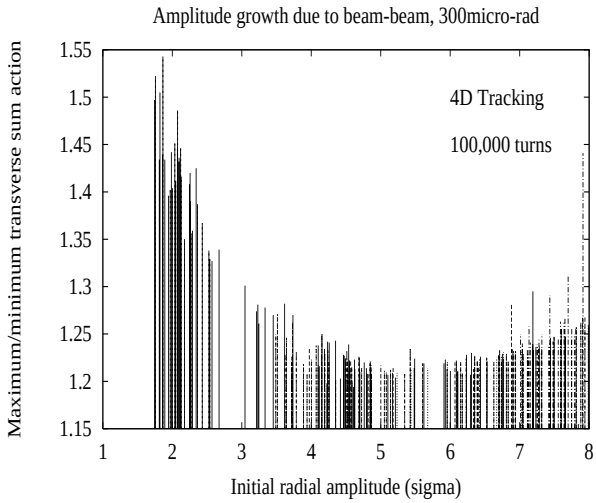

Figure 6: Relative amplitude growth with beam-beam interactions only, crossing angle of 300μrad and 4D tracking. About 400 particles were distributed with initial radial amplitudes ranging from 2 to 8 sigma and tracked for 100,000 turns. Particle excursions in this region are not very large.

To study the growth due to the beam-beam kicks, we have used initial populations of up to 500 particles distributed transversely from 2-12σ and in energy up to $3\sigma_p/p_0$. Tracking is done in both 4D and 6D phase space, the latter to examine the effects of synchrotron oscillations and energy kicks from the beam-beam interaction. For purely linear motion, the individual transverse actions would be constant in time while for nonlinear motion dominated by the coupling resonance $Q_y - Q_x = p$ (which the present tunes are close to), the sum of the transverse actions would be constant. One of the quantities that we record during tracking is the sum of the transverse actions $J_x + J_y$ for each particle at every turn. We take $(J_x + J_y)_{max}/(J_x + J_y)_{min}$ as a measure of the amplitude excursion during the tracking. The amplitude swing in units of the rms radial beam size is the square root of this quantity. We note that the physical aperture in the IR quadrupoles is limited to 15σ.

Figure 6 shows the amplitude growth of an initial distribution between 2-8σ at a crossing angle of 300μrad tracked for 10^5turns. Over this time period, 4D tracking shows that the excursion is not large for any of the particles tracked.

Figure 7 shows the maximum relative growth in action for particles between 2-8σ as a function of the crossing angle. At crossing angles below 300μrad, the amplitude growth is very large suggesting that significant numbers of particles would be lost from this distribution. The amplitude growth can be quantified by the separation between the beams. For example, at 250μrad, the beam separa-

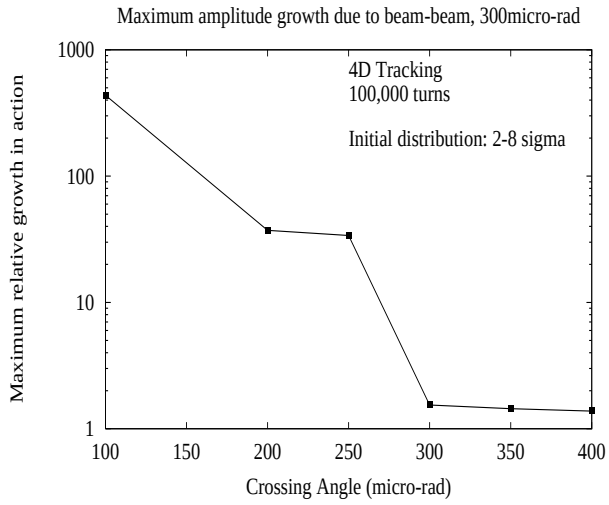

Figure 7: Maximum relative growth in the sum action due to the beam-beam interactions alone as a function of the crossing angle. The ordinate is plotted on a log scale. At each crossing angle, particles were distributed between 2-8σ. At 100μrad, the amplitude growth is very large and very few particles in the distribution will survive. The growth is significant even at 200-250μrad. At crossing angles of 300-400μrad, the largest relative growth (which is less than 2) occurs for particles in the core.

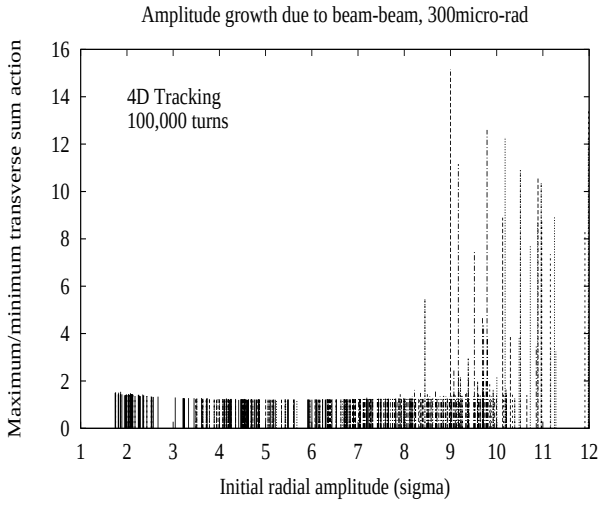

Figure 8: Similar to Figure 6 except that 500 particles were placed at initial amplitudes up to 12σ. Significant amplitude growth is observed to start at 8.5σ, the maximum swing takes this particle to an amplitude of about 20σ or beyond the physical aperture.

tion in the drifts is about 7.9σ so particles on one side of the bunch center beyond $\sim$6σ will be in the core of the other beam and will experience strong kicks. At 300μrad, the separation in the drifts is about 9.5σ and the majority of particles at amplitudes up to 8σ are further away from the core of the other beam. Hence at crossing angles of 300μrad and larger, amplitude growth is small for particles at initial amplitudes of less than 8σ.

At larger initial amplitudes, we find significant growth even at a crossing angle of 300μrad. Figure 8 shows the swing in action for a distribution of 500 particles between 2-12σ. Starting at 8.5σ, the amplitude growth is now large enough for amplitudes to exceed the physical aperture.

We have considered two different time-dependent effects. The effects of synchro-beta coupling as seen with 6D tracking are shown in Figure 9. The effects of tune fluctuations modelled by an Ornstein-Uhlenbeck spectrum with amplitude $\Delta Q = 5 \times 10^{-5}$ and a correlation time of $\tau_c = 10$turns [for a motivation and application to the LHC see [5]] with 4D tracking are shown in Figure 10. With either of these effects we find that amplitude growth beyond 7σ is greater than it is with 4D tracking alone (compare Figure 6) but at least over 10^5 turns not large enough to reach the physical aperture.

One way to avoid the amplitude growth of particles in the tails would be to increase the separation between the beams by increasing the crossing angle. Figure 11 shows that at a crossing angle of 350μrad, the amplitude growth with 4D tracking starts to be significant only for initial amplitudes

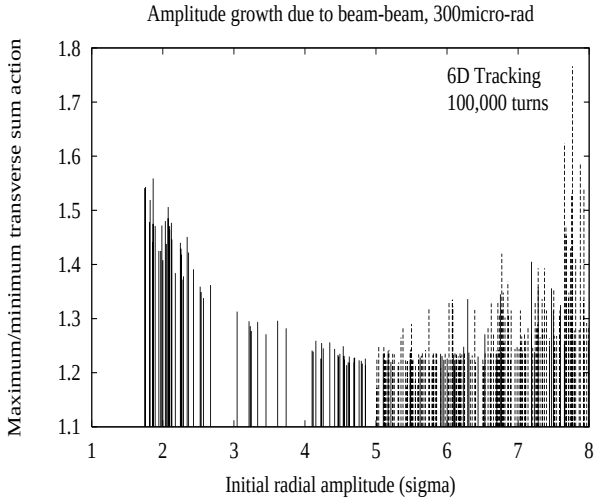

Figure 9: Amplitude growth with beam-beam interactions only and 6D tracking. 250 particles were distributed with initial amplitudes ranging from 2 to 8 sigma. Larger growth is now seen for particle amplitudes greater than 7σ when synchrotron oscillations and energy kicks due to the beam-beam are included. This figure should be compared with Figure 6.

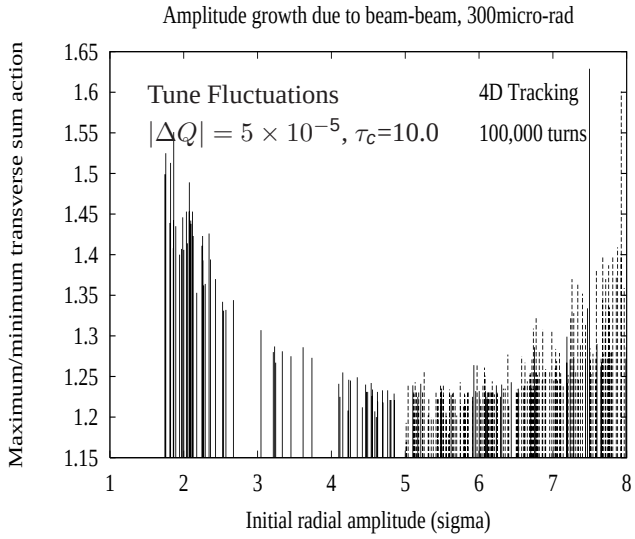

Figure 10: 4D tracking and tune fluctuations modelled by an Ornstein-Uhlenbeck spectrum [5]. Initial distribution of 250 particles between 2-8σ. As with 6D tracking we observe larger amplitude growth beyond 7σ compared to the case with only 4D tracking (cf. Figure 6).

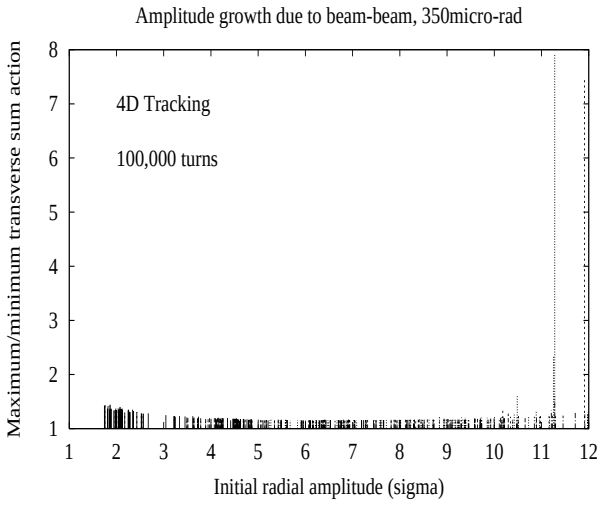

Figure 11: Same as Figure 9 but at a crossing angle of 350μrad. At this angle, significant growth is observed only at initial amplitudes greater than 11σ.

beyond 11σ.

6 CONCLUSIONS

- Dynamic aperture without beam-beam interactions. With random errors from error tables V2.0 included, mixing the Fermilab and KEK magnets is found to improve the dynamic aperture. However, the dynamic aperture with these error tables is dominated by the relatively large systematic value of $\langle b_{10} \rangle$=-0.25 in the KEK magnets. As a consequence, the KEK cross section is to be redesigned to reduce the systematic value to zero with an uncertainty on the systematic of 0.1 units. This will be reflected in V3.0 of the KEK error harmonics.

- Dynamic aperture with beam-beam interactions. Short term tracking (1000 turns) is no longer sufficient. A minimum of 10^5 turns is needed in order to determine the variation of the dynamic aperture with parameters such as the crossing angle. Tracking for 10^5 turns shows that the dynamic aperture increases as the crossing angle is increased from 100μrad to 300μrad but then falls slightly with a further increase in crossing angle. At 300μrad, the average dynamic aperture calculated at 10^5 turns and averaged over emittance space and 5 random seeds is about 9.5σ. Longer tracking studies for 10^6 turns along the diagonal in emittance space and for 2 random seeds indicate a nearly constant dynamic aperture of about 6σ at crossing angles from 300-400μrad. The choice of 300μrad therefore seems appropriate given the present error harmonics of the triplets. This may need to be re-examined if the effects of higher order harmonics, such as (b_{14}, a_{14}) which have not been included in the present study, are found to be important.

- Amplitude growth in the tails due to the beam-beam interactions only was studied with a different code but using many more particles (500) distributed between 2 and 12σ. At a crossing angle of 300μrad, there is no significant growth between 2-8σ but starting at around 8.5σ, there are large excursions suggesting that particles beyond this amplitude will not survive. When synchrotron oscillations or tune fluctuations are added, larger amplitude growth starts at around 7σ. In the absence of any time-dependent effects we find that at the larger crossing angle of 350μrad, amplitude growth is not significant for particles at initial amplitudes smaller than about 11σ.

7 REFERENCES

[1] W. Chou & D. Ritson, PAC 1997

[2] A. Russell, private communication

[3] C.H. Iselin & H. Grote, MAD, CERN/SL/90-13 (AP)

[4] N. Gelfand, LHC-AP mini workshop at FNAL (Oct 1998)

[5] T. Sen, LHC Project Report 90 (1997)